AIAA JOURNAL
Vol. 40, No. 10, October 2002

Modeling Rotating and Swirling Turbulent Flows: A Perpetual Challenge

S. Jakirlić*
Darmstadt University of Technology, D-64287 Darmstadt, Germany
K. Hanjalić†
Delft University of Technology, 2628 CJ Delft, The Netherlands
and
C. Tropea‡
Darmstadt University of Technology, D-64287 Darmstadt, Germany

Several types of rotating and swirling flows for a range of Reynolds numbers and rotation rates or swirl intensities have been studied computationally, aimed at identifying specific features that require special consideration in turbulence modeling. The flows considered include turbulent channel flows subjected to streamwise and spanwise rotation, with stationary and moving boundaries; developing and fully developed flows in axially rotating pipes; and swirling flows in combustor geometries and long pipes. Computations performed with three versions of the second-moment closure and two eddy-viscosity models show that the second-moment models are superior, especially when the equations are integrated up to the wall. Such models reproduced the main flow parameters for all flows considered in acceptable agreement with the available experimental data and direct numerical simulations. However, challenges still remain in predicting accurately some specific flow features, such as capturing the transition from a free vortex to solid-body rotation in a long straight pipe with a weak swirl, or reproducing the normal stress components in the core region. Also, the so-called $\overline{uw}$ anomaly in fully developed flows with streamwise rotation remains questionable. For rotating flows, the low-Reynolds-number models yield a somewhat premature flow relaminarization at high rotation speeds.

I. Introduction

TOGETHER with flow separation, swirl and rotation are probably the most frequently encountered flow phenomena in technical applications: aircraft gas combustors, pulverized coal burners, turbomachinery, cyclone separators, centrifugal gas separators, large-scale pipeline systems, etc. Because of their practical and theoretical importance, numerous experimental investigations, computational modeling and, more recently, direct numerical simulations (DNS) and large-eddy simulations (LES) of these flows have been reported in the literature. We mention here only some relevant publications on several flow classes: pipe flows rotating about their own axis,[1–12] rotating channel flows with stationary[9,13–20] and moving boundaries,[20,21] and swirling flows in geometries relevant to combustor chambers[10,22–27] and long pipes.[27–29] Although experimental and DNS/LES studies provide useful information and insight into the flow physics, the computational methods involving turbulence modeling offers the broadest prospects for industrial applications. However, the complex flow structure invalidates some of the assumptions on which simple turbulence models are based. Particularly challenging for modeling are flow features that are absent in simple flows in which the models are usually tuned and validated. Examples of such features are the secondary shear strain, for example, the shear component $\partial W/\partial r$ in addition to the common mean shear $\partial U/\partial r$, streamline curvature (with respect to the additional strain $-W/r$), strong departure from local energy equilibrium, and the effects of turbulence anisotropy. In flows with system rotation, the flow structure is additionally modified due to the action of Coriolis and centrifugal forces.

We report here on the investigation of several flow classes that exhibit the specific flow features mentioned. The choice of the flows was determined by their industrial relevance, but also by the availability of experimental and/or DNS data for model validation. The following flow categories were considered: developing (experimental[1]) and fully developed flows in an axially rotating pipe (DNS[5–7]), swirling flows in short (combustor) geometries (experimental[22,23]) and in long pipes (experimental[28,29]), channel flows with streamwise (DNS[15]) and spanwise rotation with stationary (rotating Poiseuille flow, DNS,[14] LES,[16] and experimental[13] and moving walls (rotating Couette flow, DNS[21]). The rotating channel flows and the Roback and Johnson's,[22] swirling flow served as the test cases in the seventh–ninth European Research Community on Flow, Turbulence and Combustion (ERCOFTAC) workshops on refined turbulence modeling. Schematic representation of all cases considered is shown in Fig. 1.

It is well known that the standard k–ε and other linear two-equation eddy-viscosity models have a number of weaknesses, which are especially pronounced in flows affected by rotation and swirl. In contrast, second-moment closures, which provide information about all stress components and contain exact terms for rotation effects in the stress equation, are inherently capable of capturing most of the phenomena mentioned earlier. Indeed, in contrast to the k–ε models, in all flow cases reported here the second-moment closures produced acceptable results. However, a systematic scrutiny of a large range of flows revealed several specific shortcomings: the wrong (negative) sign of the $\overline{uw}$ shear stress component, the tangential velocity profile retains its initial concentrated vortex shape too long in a long straight pipe with a weak swirl, and the premature flow laminarization in axially rotating pipes and cylinders. Although usually not detrimental, these shortcomings pose intriguing challenges to turbulence modeling and may also be of importance for accurate prediction of engineering flow parameters, especially at high rotation rates and swirl intensities.

The main goal of this work is to provide a systematic survey of the performance of selected second-moment closures in a range of rotating and swirling flows and to establish more clearly their

Received 30 January 2001; revision received 10 January 2002; accepted for publication 23 May 2002.

*Research Scientist, Chair of Fluid Mechanics and Aerodynamics, Petersenstr. 30.
†Professor, Faculty of Applied Physics, Lorentzweg 1.
‡Professor, Chair of Fluid Mechanics and Aerodynamics, Petersenstr. 30. Member AIAA.

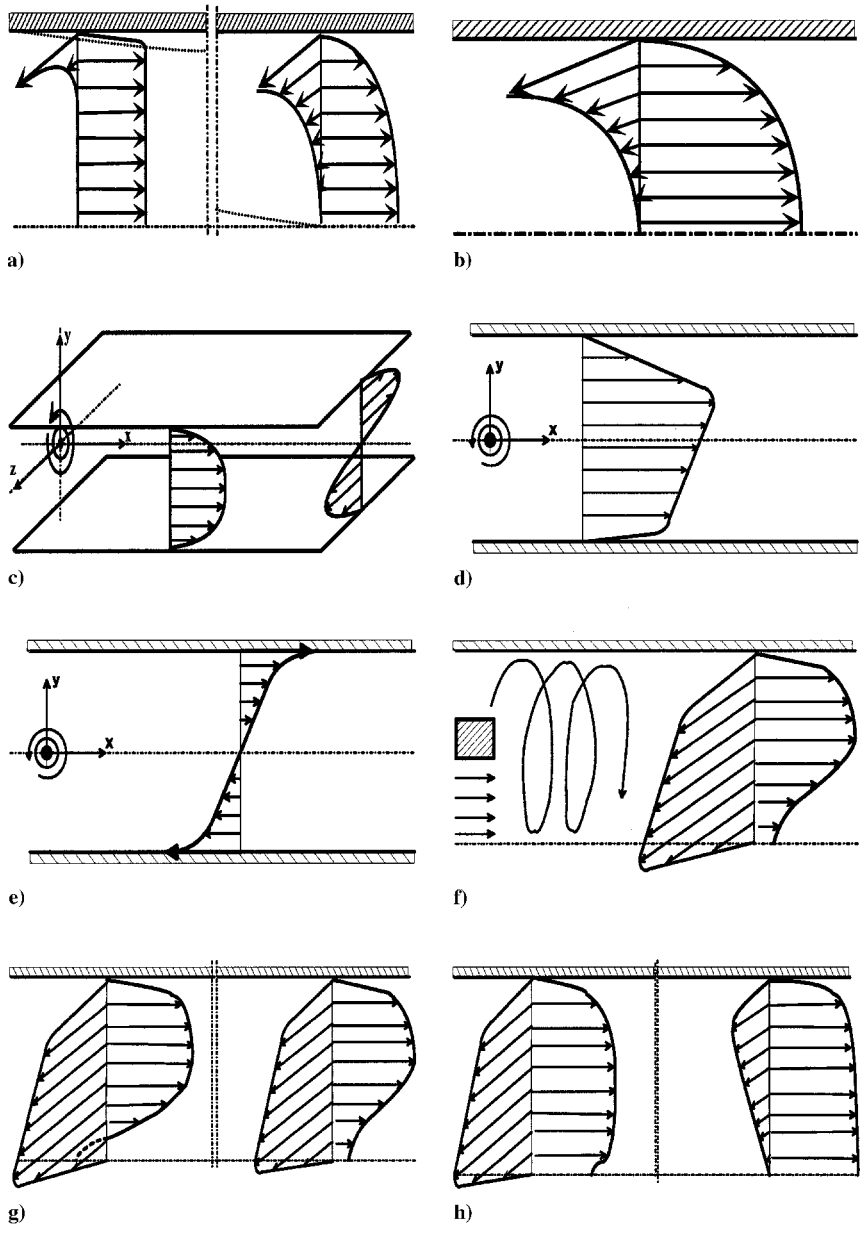

Fig. 1 Schematic of the flow configurations considered: a) developing rotating pipe flow, b) fully developed rotating pipe flow, c) channel flow with streamwise rotation, d) channel flow with spanwise rotation, e) rotating Couette flow, f) swirling flow in a combustor chamber, g) strong swirl in a long straight pipe, and h) weak swirl in a long straight pipe.

potential and limitations, particularly in comparison with linear eddy-viscosity models. The study also provides further insight into the physics of system rotation, swirl, transverse shear, and their effect on turbulence, within the framework of the Reynolds averaged Navier–Stokes (RANS) approach, as well as ideas for possible model improvement. The suitability of the wall function approach for treating the near-wall region is also discussed.

II. Numerical Method and Turbulence Models

The flows considered are essentially all three dimensional (except the two-dimensional channel flows rotating in orthogonal mode), for which all three velocity components and all six Reynolds stress components must be accounted for. However, the Reynolds averaged continuity and momentum equations are solved with assumption of axisymmetry ($\partial/\partial\varphi = 0$):

$$\frac{1}{r}\frac{\partial(rU_j)}{\partial x_j} = 0 \tag{1}$$

$$\frac{1}{r}\frac{\partial(rU_j\boldsymbol{U}_i)}{\partial x_j} = \frac{1}{r}\frac{\partial}{\partial x_j}\left[r\left(\nu\frac{\partial \boldsymbol{U}_i}{\partial x_j} - \overline{u_i u_j}\right)\right] - \frac{1}{\rho}\frac{\partial P}{\partial \boldsymbol{x}_i} + S_{U_i} \tag{2}$$

Table 1 Sources in mean momentum equations

S_{U_i}	Convection	Viscous transport	Turbulent transport
S_U	—	—	$-\overline{uv}/r$
S_V	$+W^2/r$	$-\nu V/r^2$	$+\overline{w^2}/r$
S_W	$-VW/r$	$-\nu W/r^2$	$-\overline{wv}/r$

where the vector $\boldsymbol{x}_i(r, z)$ denotes the coordinate directions and $\boldsymbol{U}_i(U_r, U_\varphi, U_z)$ $[\equiv(V, W, U)]$ is the mean velocity vector. The source terms S_{U_i}, arising from the coordinate transformation, are given in Table 1.

All computations were performed by a computer code based on a finite volume numerical method for solving the RANS equations in orthogonal coordinate systems with a collocated variable arrangement. (See Jakirlić et al.[30] for more details.) For discretization of the convective fluxes, a blended upwind-central differencing scheme, implemented in the so-called deferred-correction manner was used. For most flows considered, we used a high portion of central differencing (CD): The blending factor was typically between 0.7 and 1.0 for all variables. Because of a weak flow-to-grid skewness, and because of the very fine grid used, in most

Table 2 Grids and dimensions of the solution domains for the flows computed

Flow type	Grid (control volumes)		Solution domain	
	High-Reynolds-number model	Low-Reynolds-number model	Length L, mm	Radius R, mm Width $2h$, mm
Flows in axially rotating pipes				
Ref. 4 (experiment), Refs. 5–7 (DNS)				
$Re_m = 4.9 \times 10^3$–2×10^4; $N = 0.0$–10.0	2×20–40	2×60–100	2	100
Ref. 1 (experiment)			6000	
$Re_m = 6 \times 10^4$; $N = 0.0, 0.5, 0.83$	100×70	100×130	(L of rotating part = 4120)	50
Flows in rotating channels				
Pouseuille flow with spanwise rotation: Ref. 14 (DNS)				
$Ro = 0.0$–0.5	10×40	10×120	10	200
Couette flow with spanwise rotation: Ref. 21 (DNS)				
$Ro = 0.0$–0.5	10×40	10×120	10	200
Channel with streamwise rotation: Ref. 15 (DNS)				
$Ro_\tau = 0.0$–10.0	2×40	2×120	2	200
Swirling flows in combustor chambers				
Ref. 23 (experiment) $S = 2.25$	100×70	100×130	348	62.5
Ref. 22 (experiment) $S = 0.45$	200×70	220×120	750	61
Swirling flows in long straight pipes				
Ref. 28 (experiment) $Re_m = 5 \times 10^4$, $S = 1.0$	200×60	200×140	6150	75
Ref. 29 (experiment) $Re_m = 5 \times 10^4$, $S = 0.1$	120×60	120×100	5300	35

Table 3 Summary of the model coefficients

Parameter	GL	SSG	HJ
C_1	1.8	1.7	$2.5AF^{\frac{1}{4}}f + A^{\frac{1}{2}}E^2$
C_1'	0.0	1.05	0.0
C_1''	0.0	0.9	0.0
C_3	0.8	0.8–$0.65\,A_2^{\frac{1}{2}}$	$1.067\,A^{\frac{1}{2}}$
C_4	0.6	0.625	$0.8\,A^{\frac{1}{2}}$
C_5	0.6	0.2	$0.8\,A^{\frac{1}{2}}$
C_1^w	0.5	0.0	$\max(1 - 1.75AF^{\frac{1}{4}}f; 0.3)$
C_2^w	0.3	0.0	$\min(A; 0.3)$
α	1.0	1.0	1.4
C_s	0.22	0.22	0.22
f_s	0.0	0.0	$1 - A^{\frac{1}{2}}E^2$
C_{ε_1}	1.44	1.44	1.44
C_{ε_2}	1.92	1.83	1.92
C_ε	0.18	0.18	0.18
$\tilde{\varepsilon}$	ε	ε	$\tilde{\varepsilon}$
f_ε	1.0	1.0	$1 - \frac{C_{\varepsilon_2} - 1.4}{C_{\varepsilon_2}} \exp\left\{-\left(\frac{Re_t}{6}\right)^2\right\}$
S_ε	0	0	$0.25\nu\frac{k}{\varepsilon}\overline{u_j u_k}\frac{\partial^2 U_i}{\partial x_j \partial x_l}\frac{\partial^2 U_i}{\partial x_k \partial x_l}$

cases the solutions are virtually indistinguishable from those obtained by pure upwind differencing. [The only exception was the swirling flow discharging into a sudden expansion (experiment discribed by Roback and Johnson[22]).] The solution domain used for the computation of the swirling flows and of the flows in an axially rotating pipe/cylinder typically has the shape of the axisymmetric pipe geometry, with a length L and a height $R = D/2$, D being a pipe, that is, combustor diameter. (See Table 2 for dimensions of the solution domain and sizes of the numerical grids used.) For rotating channel flows, it was necessary to account for both walls. In the case of fully developed flows, periodic inlet/outlet boundary conditions were applied.

Computations were performed with several two-equation models: the standard k–ε high-Reynolds-number model and with its two low-Reynolds-number extensions, due to Launder and Sharma[31] (LS) and Chien,[32] as well as with three types of Reynolds stress models: 1) the basic high-Reynolds-number version [see Gibson and Launder[33] (GL)], 2) the model of Speziale et al.[34] (SSG), and 3) the low-Reynolds-number version of the second-moment (Reynolds stress) closure model (RSM) denoted as the Hanjalić–Jakirlić (HJ) low-Reynolds-number RSM. The latter model contains the modifications for viscosity and wall blockage effects. (See Hanjalić and Jakirlić[35] for more details.) A summary of the model coefficients is given in Table 3.

The second-moment closure models are defined by the transport equations for the turbulent stress tensor and turbulence energy dissipation (for equations in cylindrical coordinates, see Jakirlić et al.[30]):

$$\frac{\partial}{\partial x_k}(U_k\overline{u_i u_j}) = \frac{\partial}{\partial x_k}\left[\left(\nu\delta_{kl} + C_s\frac{k}{\varepsilon}\overline{u_k u_l}\right)\frac{\partial\overline{u_i u_j}}{\partial x_l}\right] - \overline{u_i u_k}\frac{\partial U_j}{\partial x_k} - \overline{u_j u_k}\frac{\partial U_i}{\partial x_k} + \Phi_{ij} - \varepsilon_{ij} \tag{3}$$

$$\frac{\partial}{\partial x_k}(U_k\varepsilon) = \frac{\partial}{\partial x_k}\left[\left(\nu\delta_{kl} + C_\varepsilon\frac{k}{\varepsilon}\overline{u_k u_l}\right)\frac{\partial\varepsilon}{\partial x_l}\right] - C_{\varepsilon_1}\frac{\varepsilon}{k}\left(\overline{u_k u_l}\frac{\partial U_k}{\partial x_l}\right) - C_{\varepsilon_2}f_\varepsilon\frac{\varepsilon\tilde{\varepsilon}}{k} + S_\varepsilon \tag{4}$$

A major difference between various second-moment closure models is in the treatment of the pressure strain term Φ_{ij} and the stress dissipation rate ε_{ij}:

$$\begin{aligned}\Phi_{ij} = {} & -C_1\varepsilon a_{ij} + C_1'\varepsilon\left[a_{ik}a_{kj} - \tfrac{1}{3}A_2\delta_{ij}\right] \\ & - C_2'P_k a_{ij} + C_3 k S_{ij} + C_4 k\left[a_{ik}S_{jk} + a_{jk}S_{ik} - \tfrac{2}{3}\delta_{ij}a_{kl}S_{kl}\right] \\ & + C_5 k(a_{ik}W_{jk} + a_{jk}W_{ik}) \\ & + C_1^w f_w(\varepsilon/k)\left[\overline{u_k u_m}n_k n_m\delta_{ij} - \tfrac{3}{2}\overline{u_i u_k}n_k n_j - \tfrac{3}{2}\overline{u_k u_j}n_k n_i\right] \\ & + C_2^w f_w\left[\Phi_{km,2}n_k n_m\delta_{ij} - \tfrac{3}{2}\Phi_{ik,2}n_k n_j - \tfrac{3}{2}\Phi_{kj,2}n_k n_i\right]\end{aligned} \tag{5}$$

$$\varepsilon_{ij} = f_s\varepsilon_{ij}^* + (1 - f_s)\tfrac{2}{3}\delta_{ij}\varepsilon \tag{6}$$

where

$$\varepsilon_{ij}^* = \frac{(\varepsilon/k)[\overline{u_i u_j} + (\overline{u_i u_k}n_j n_k + \overline{u_j u_k}n_i n_k + \overline{u_k u_l}n_k n_l n_i n_j)f_d]}{1 + \frac{3}{2}(\overline{u_p u_q}/k)n_p n_q f_d}$$

Of course, in the high-Reynolds-number models, $f_s = 0$ so that Eq. (6) reduces to $\varepsilon_{ij} = 2\varepsilon\delta_{ij}/3$. The model coefficients are shown in Table 3, and the functions are as follows:

$$f_w = \min\left\{\frac{k^{\frac{3}{2}}}{2.5\varepsilon x_n}; \alpha\right\}, \qquad f_d = (1 + 0.1Re_t)$$

$$F = \min\{0.6; A_2\}, \qquad f = \min\left\{\left(\frac{Re_t}{150}\right)^{\frac{3}{2}}; 1\right\}$$

$$A = 1 - \frac{9}{8}(A_2 - A_3), \qquad A_2 = a_{ij}a_{ji}$$

$$A_3 = a_{ij}a_{jk}a_{ki}, \qquad a_{ij} = \frac{\overline{u_i u_j}}{k} - \frac{2}{3}\delta_{ij}, \qquad Re_t = \frac{k^2}{\nu\varepsilon}$$

$$S_{ij} = \frac{1}{2}\left(\frac{\partial U_i}{\partial x_j} + \frac{\partial U_j}{\partial x_i}\right), \qquad E = 1 - \frac{9}{8}(E_2 - E_3)$$

$$E_2 = e_{ij}e_{ji}, \qquad E_3 = e_{ij}e_{jk}e_{ki}, \qquad e_{ij} = \frac{\varepsilon_{ij}}{\varepsilon} - \frac{2}{3}\delta_{ij}$$

$$\tilde{\varepsilon} = \varepsilon - 2\nu\frac{\partial\sqrt{k}}{\partial x_j}\frac{\partial\sqrt{k}}{\partial x_j}, \qquad W_{ij} = \frac{1}{2}\left(\frac{\partial U_i}{\partial x_j} - \frac{\partial U_j}{\partial x_i}\right)$$

In the remainder of the paper we present a summary of selected results, focusing on the specific effects discussed earlier and the performance of different models in reproducing those effects.

III. Discussion

Logarithmic Law

It is well known that swirl and rotation cause a strong deviation of the velocity profile from the logarithmic law, invalidating the standard wall functions for the treatment of the wall boundary condition. In such cases it seems unavoidable to use a turbulence model that accounts for low-Reynolds-number and wall-proximity effects, allowing integration of the governing equations up to the wall. This is especially the case in flows in axially rotating pipes and cylinders, which are prone to laminarization. This is shown in Figs. 2, 3a, and 4, where the computed velocity profiles are compared with the semilogarithmic line and with the available DNS and experimental data for the flow in an axially rotating pipe, for the swirling flow in a long straight pipe and the rotating Poiseuille and Couette flows.

For axially rotating pipe flows, we show results for a range of rotation rates, defined by the ratio of the circumferential wall velocity W_{wall} to the axial bulk velocity U_b, $N = W_{\text{wall}}/U_b$. The DNS shows that the axial velocity $U^+ = U/U_\tau$ follows the logarithmic slope for the lower rotation rates but departs at higher rotation rates (Fig. 2a). However, the circumferential velocity ($W^+ = |W_{\text{wall}} - W|/W_\tau$) shows no similarity with the logarithmic law. The computations using the HJ model reproduce this behavior well (Fig. 2a). Figure 2b shows the mean resultant velocity $R^+ = (U^{+2} + W^{+2})^{1/2}$ computed by the basic high-Reynolds-number, second-moment closure model[33] using wall functions. Whereas the computations of the cases with lower rotation rates ($N < 1.0$; here $N = 0.32$ shown) result in good agreement with DNS data, the inadequacy of the wall function concept becomes visible at higher rotation rates ($N \geq 1.0$; here $N = 2.0$ shown). Note that the velocity gradient in the first near-wall grid point is prescribed to $\mathrm{d}U/\mathrm{d}y = U_\tau/(\kappa y)$ by applying the wall functions (Fig. 2b).

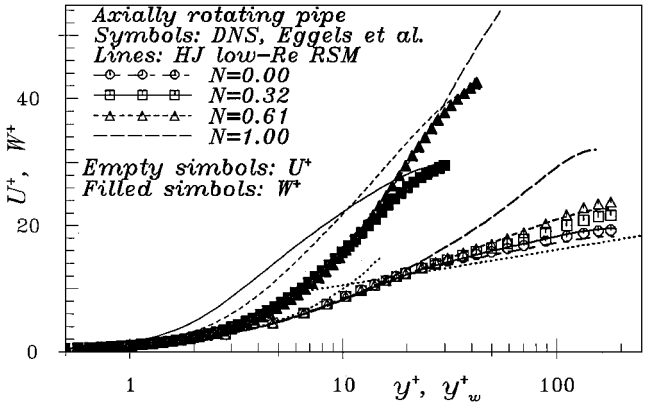

Fig. 2 Departure of the mean axial U^+, circumferential W^+, and the resultant R^+ velocity from the logarithmic law for the flow in an axially rotating pipe.

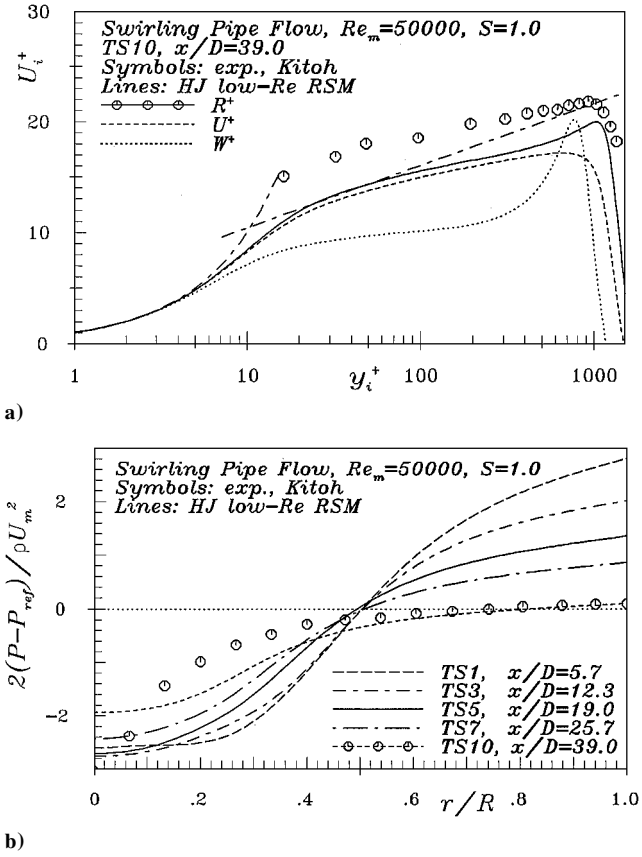

Fig. 3 a) Departure of the mean axial U^+, circumferential W^+, and the resultant R^+ velocity from the logarithmic law and b) pressure profiles at selected positions in the swirling flow in a long straight pipe.

The ratio of the turbulent kinetic energy production to its dissipation rate is presented in Fig. 5 for both rotation rates computed. In both cases, the equilibrium value $P_k/\varepsilon \approx 1$ was taken at the node closest to the wall, as follows from the wall function concept. Whereas for $N = 0.32$ this value of unity holds almost up to $y^+ \approx 100$, in accordance to DNS data, this is not the case for $N = 2.0$. The ratio drops suddenly to a very low value, leading finally to zero turbulent kinetic energy production in the remainder of the cross section, in spite of using the fixed turbulent boundary condition.

The shape of the resultant velocity profile in a strongly swirling flow in a long pipe (Fig. 3a) shows a behavior that suggests opposite signs of the streamwise pressure gradient in the annular (wall) and core flow regions (Fig. 3b). In the annular region, the pressure gradient is favorable, influencing the velocity profile in such a way that it overshoots the log-line at the edge of the buffer zone, similar to the behavior encountered in accelerated flows. Contrary to this, the flow in the core region is decelerated, indicating the existence of an adverse pressure gradient. [The disagreement with experimental results corresponds closely to the disagreement of both the normal-to-the-wall and spanwise stress components in this flow region (for example, see Fig. 6a), $\partial P/\partial r = \rho[\partial(-r\overline{v^2})/\partial r + W^2 + \overline{w^2}]/r$.]

Figure 4 shows the semilog profiles of the mean axial velocity in the channel flows rotating about the orthogonal axis, with stationary

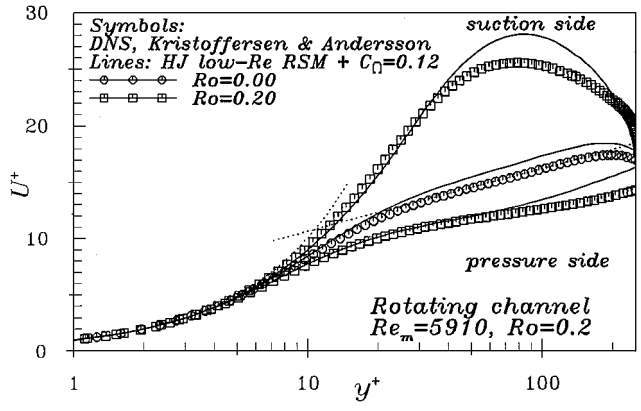

a)

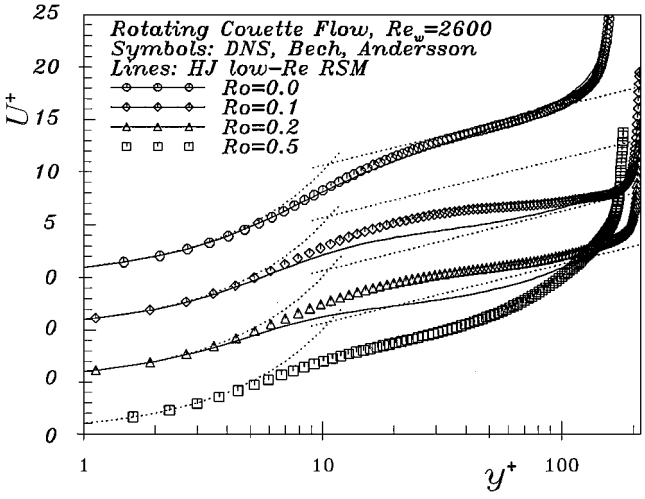

b)

Fig. 4 Departure of the mean axial U^+ velocity from the logarithmic law for the rotating a) Poiseuille and b) Couette flows.

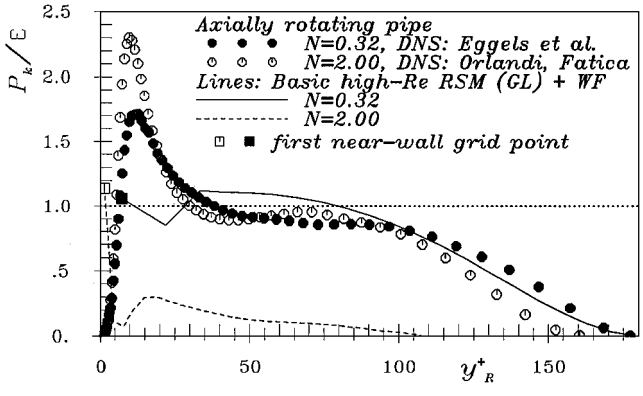

Fig. 5 Ratio of the kinetic energy production to its dissipation rate for the flow in an axially rotating pipe.

(Fig. 4a) and moving walls (Fig. 4b). On the suction side of the rotating Poiseuille flow (Fig. 4a), the rotation has a stabilizing effect on turbulence, as indicated by a positive $S = -2\Omega/(\partial U/\partial y) > 0$, where $\Omega_i(0, 0, \Omega)$ is the system vorticity and $\partial U/\partial y$ represents the local mean shear vorticity. Here the velocity profile exhibits a laminarlike shape, approaching the linear law ($U^+ = y^+$) with increasing bulk rotation number $Ro = 2\Omega h/U_b$, where h is a half channel width. The velocity profile in the lower half of the channel (pressure side, with a destabilizing effect on turbulence, $S < 0$) lies completely below the log-law profile.

For rotating Couette flow (Fig. 4b, $Ro = 2\Omega h/U_{\text{wall}}$), the deviation of the velocity profile from the log-law is also obvious. Unlike the rotating channel with stationary walls, the ratio S is always negative, implying a continuous destabilizing effect on turbulence. The

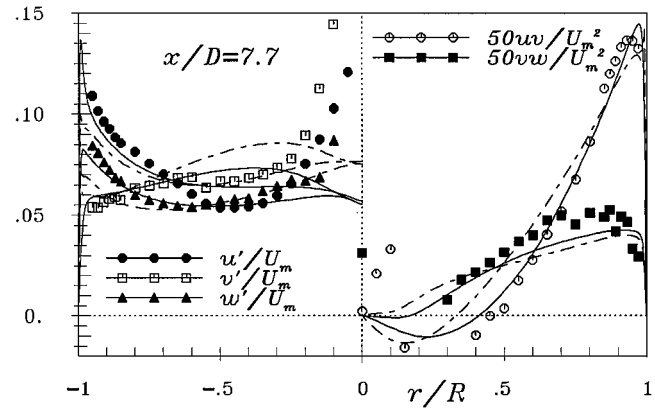

a)

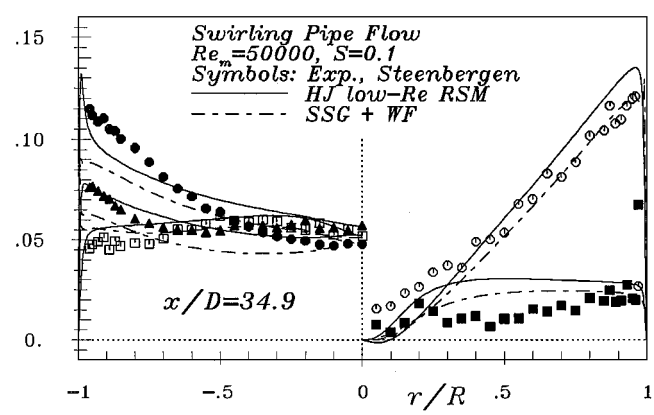

b)

Fig. 6 Profiles of the Reynolds stress components at selected positions in the swirling flow in a long, straight pipe (experiment of Steenbergen[29]).

rotation rates presented do not exhibit a laminarlike profile as in the earlier case despite the decay of turbulent stress components observed (Fig. 7b). (See the works of Pettersson and Andersson[20] and Bech and Andersson[21] for further details.) Because of this transitional nature, the wall functions are here totally unsuitable.

Fully Developed Channel Flows Rotating in Orthogonal Mode

Turbulent flow in a channel, rotating around a spanwise axis z, represents an idealization of the flow in blade passages of radial flow pumps and compressor impellers. These flows are commonly considered in the rotating frame of reference. In that case, one has to account for the exact production of turbulent stresses $R_{ij} = -2\Omega_k(\overline{u_j u_m}\epsilon_{ikm} + \overline{u_i u_m}\epsilon_{jkm})$. Furthermore, the model of the redistribution among the Reynolds stress components needs to be modified to account for body forces originating from system rotation.[17] For the case considered here with constant angular velocity $\boldsymbol{\Omega}(0, 0, \Omega)$), these are as follows.

Coriolis force:

$$-2\rho\boldsymbol{\Omega} \times \boldsymbol{U}(2\rho\Omega V, -2\rho\Omega U, 0) \tag{7a}$$

Centrifugal force:

$$-\rho\boldsymbol{\Omega} \times (\boldsymbol{\Omega} \times \boldsymbol{x})(-\rho\Omega^2 x, -\rho\Omega^2 y, 0) \tag{7b}$$

where the vector $\boldsymbol{x}(x, y, z)$ denotes the coordinate directions and $\boldsymbol{U}(U, V, 0)$ is the mean velocity vector in the rotating frame of reference. Both forces act on the mean flow inducing a secondary motion and on turbulence, modifying its structure. This recirculating motion (roll cells) is particularly intensive if the channel walls are moving (rotating Couette flows). Both flow cases, with stagnant and moving walls, were recently investigated by DNS by Kristoffersen and Andersson[14] and Bech and Andersson.[21] Several rotational intensities, expressed in terms of rotation number Ro ranging between 0.0 and 0.5, were considered, all at relatively low bulk Reynolds numbers, $Re_m = Re_b = U_b 2h/\nu \approx 6000$, that is,

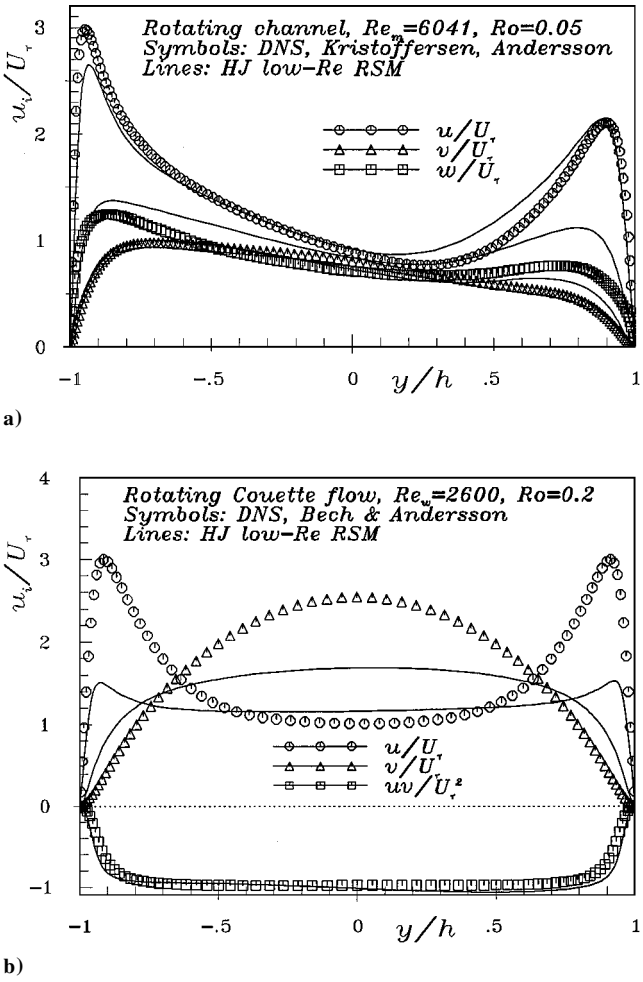

Fig. 7 Turbulence stress components in the channel flows with spanwise rotation with a) stationary and b) moving walls.

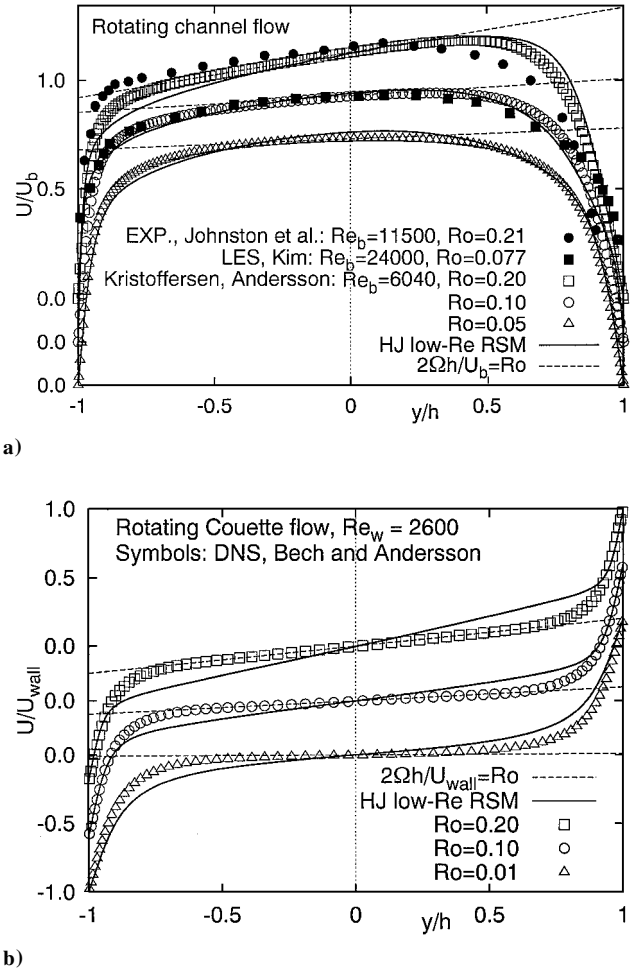

Fig. 8 Mean axial velocity profiles in the channel flows with spanwise rotation with a) stationary and b) moving walls.

$Re_w = U_{\text{wall}}h/\nu = 2600$. The RANS computations of the rotating channel flows at such a low Reynolds number show premature laminarization[18,19] as compared with DNS, which for the rotating Poiseuille flow shows that the onset of laminarization on the suction channel side occurs at $Ro = 0.5$. The introduction of a new, system-rotation related term in the dissipation equation cured this deficiency. (See section about model modifications.) At the higher Reynolds numbers investigated experimentally by Johnston et al.[13] and by Kim[16] using LES, which are much closer to the conditions encountered in turbomachinery [where Reynolds number based on the blade cord length c is about $Re_c = 10^5 - 10^6$ (e.g., Mayle[36])], there was no necessity to introduce such a term, at least for the rotation rates considered.

Figure 8 shows axial mean velocity profiles for both channel flows, with and without wall movement for different rotation rates, but also for different bulk Reynolds numbers. The influence of rotation on the profile shape is obvious, making it increasingly asymmetric with an increasing in rotational intensity. Over a portion of the channel cross section, the profiles are linear, with a (normalized) slope corresponding to the actual rotation number Ro. This is in compliance with the theory for symmetries in inhomogeneous turbulent shear flows, which yields $U = C_5\Omega y + C_6$, with C_5 and C_6 denoting the integration constants.[37] The width of this region increases at higher values of Ro. It is clear from the results presented in Figs. 8 that the model computations result in an overprediction of the mean shear rate in the channel core (corresponding to the slope of velocity profile), indicating a larger influence of rotation, which can consequently lead to premature flow laminarization.

The excessive influence of rotation on the model results is particularly visible in turbulence intensities, and especially for the rotating Couette flow (Fig. 7). The model results show much lower turbulence levels then computed by DNS (Fig. 7b). Similar results were obtained by application of the Ristorcelli, Lumley, and Abid second-moment closure model in the framework of Durbin's elliptic relaxation method (see Pettersson and Andersson[20]). In addition to possible model deficiencies, this discrepancy with DNS results can be partly ascribed to the computational procedure used. Whereas the DNS accounted for a very strong, rotationally induced secondary motion[14,21] (crossflow and streamwise secondary flow), whose turbulence intensity is much higher for the Couette flow than in the Poiseuille flow, the steady RANS method assumed that the mean motion is unidirectional.

Laminarization Phenomena in an Axially Rotating Pipe Flow

The most interesting issues in flows in rotating pipes/cylinders are the change in stress anisotropy and flow laminarization. A number of experimental investigations of fully developed and developing flows in an axially rotating pipe can be found in the literature. From the measurements of mean velocity, Nishibori et al.[2] and Hirai et al.[3] observed changes in mean flow properties, which indicated a tendency toward flow laminarization. The stabilizing effect of the positive gradient of the tangential velocity in the radial direction, corresponding to the positive Richardson number

$$Ri = \frac{2(W/r^2)\partial(rW)/\partial r}{(\partial U/\partial r)^2 + [r\partial(W/r)/\partial r]^2}$$

reduces the turbulence level, producing, in turn, a decrease in the gradient of the axial velocity component close to the wall and a consequent reduction in the friction coefficient. The centerline velocity U_{CL} increases with an increase in the rotation intensity and the velocity profile approaches the laminar form: $U_{\text{CL}} \approx 2U_{\text{bulk}}$ (Fig. 9a). According to Nishibori et al.,[2] this process is completed when the rotation rate reaches the value $N \approx 3.5$. The computation of these flows

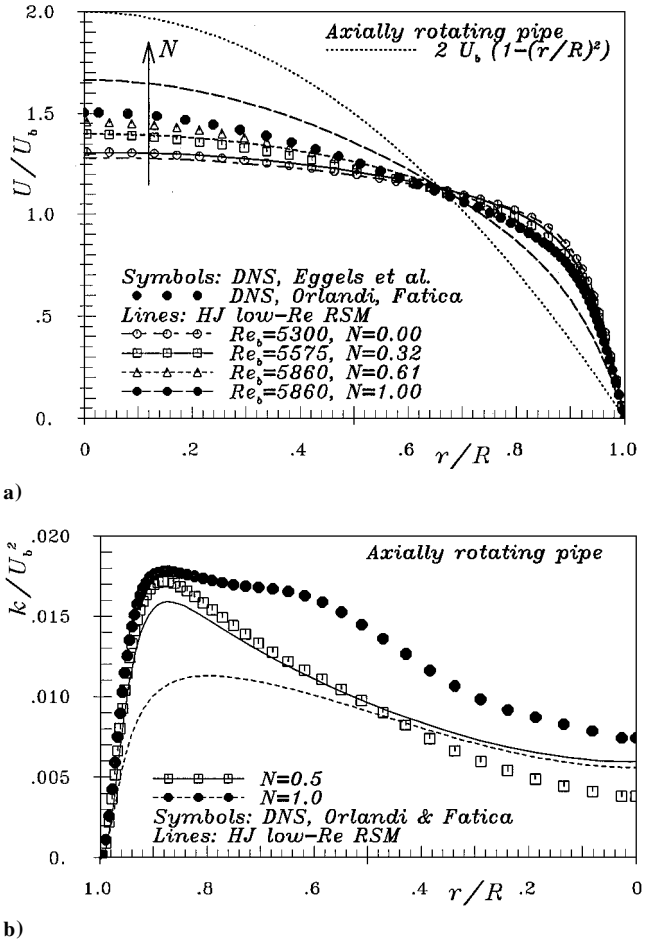

Fig. 9 Evolution of a) the axial velocity and b) kinetic energy profiles in an axially rotating pipe.

using the low-Reynolds-number Reynolds stress model supports this tendency (Fig. 9a, lines), but the laminar solution is obtained at much lower rotation rates, already at $N \approx 1.0$. An illustrative example is given in Fig. 9b, where the kinetic energy profiles for two rotation rates $N = 0.5$ and 1.0 are shown. Whereas the former agrees reasonably well with the DNS data of Orlandi and Fatica,[6] the latter shows a much lower turbulence level. For any higher rotation rate, the model computations show complete laminarization. The same outcome was observed by other authors using different low-Reynolds-number eddy viscosity model (EVM) and RSM, as reported, for example, by Shih et al.[10] (nonlinear k–ε model), Pettersson et al.[11] (second-moment closure with Durbin's elliptic relaxation method), and Poroseva et al.[12] (structure-based model). Recently, Orlandi and Ebstein[7] performed DNS for rotation rates up to $N = 10$. In spite of a close resemblance of the mean axial velocity profile to the laminar shape, the process of laminarization is, contrary to work of Nishibori et al.,[2] still not complete. The turbulence stresses, although strongly modified, show considerable levels.

The failure of all models to reproduce the laminarization at the appropriate rotation intensity indicates a deficiency in the current turbulence models. The premature flow laminarization is closely connected to the negative (false) sign of the $\overline{uw}$ stress component, causing also a negative production rate of the $\overline{uv}$ shear stress: $P_{12} - C_{12} = 2\overline{uw}W/r$. (See section about $\overline{uw}$ anomaly.) DNS computations of fully developed flow in an axially rotating pipe by Orlandi and Fatica[6] and Orlandi and Ebstein[7] for rotation rates up to $N = 10$, provide more details about the turbulent stress field and shed more light on the actual process of turbulence field modification due to rotation.

Stress Anisotropy

The DNS results also show a weakening of the stress anisotropy with an increase in the rotation speed, in particular in the near-wall region outside the viscous zone. This is clearly indicated by an increase in Lumley's two-componentality factor $A = 1 - \frac{9}{8}(A_2 - A_3)$ (Fig. 10a). The weakening of the stress anisotropy was also confirmed by Ferziger and Shaanan.[38] The peak stress component normal to the rotation plane (streamwise direction) shows a continuous decrease, whereas the components in the plane of rotation (especially the spanwise one) are enhanced, implying in fact a trend toward equalization of stress components. Very close to the wall, where the wall-normal stress diminishes faster and the turbulence approaches the two-component (2-C) limit for all five rotation rates considered, the turbulence field shows a clear tendency toward the 2-C isotropic state, as shown by symbols in the Lumley's invariant map ($II = -A_2/8$, $III = A_3/24$) (Fig. 10b). Along the straight line ($A = 0 \Rightarrow A_2 = A_3 + \frac{8}{9}$) the turbulence also has two components but is generally anisotropic. This feature is beyond the reach of any eddy-viscosity models, but surprisingly, nor can it be fully reproduced by the second-moment closures, despite satisfactory prediction of the stress anisotropy in nonrotating wall flows at different pressure gradients (e.g., Hanjalić et al.[39]). This indicates a deficiency in the pressure-redistribution model to account for the rotation effects.

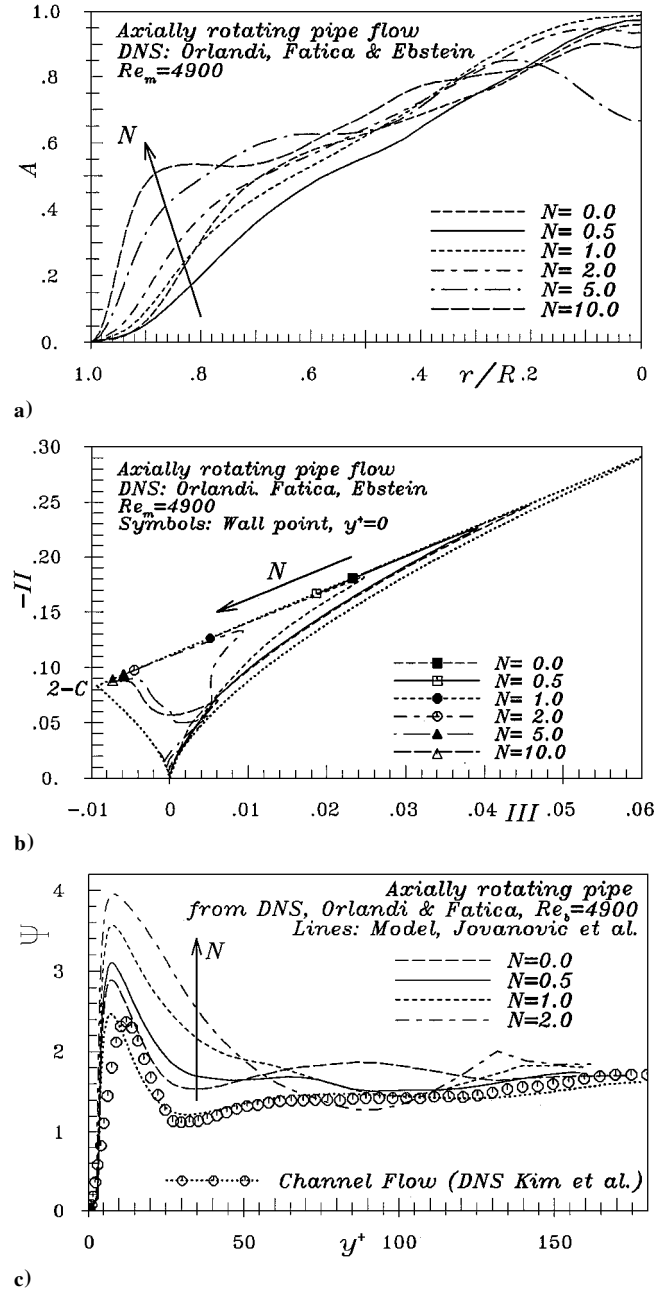

Fig. 10 Two-componentality factor, invariant map, and evolution of the coefficient $\Psi = f_\varepsilon C_{\varepsilon 2}$ in an axially rotating pipe.

Another interesting finding in the axially rotating pipe flows is the modification of the destruction term in the dissipation equation

$-\Psi\varepsilon^2/k$. Note that $\Psi = C_{\varepsilon 2} f_\varepsilon$ in conventional notation. It has already been shown for homogeneous rotating turbulence, where no production of dissipation exists,[40] that Ψ is affected by the rotation. On the other hand, the DNS of nonrotating channel flow[41] shows also a strong modification of Ψ in the near-wall region, where the turbulence approaches the 2-C state (Fig. 10c; symbols). Note that in all cases $\Psi = 0$ at the wall:

$$\Psi = -\left[\left(P_\varepsilon^4 - Y\right)\Big/\varepsilon^2/k\right] \propto y^4 \tag{8}$$

where $(P_\varepsilon^4 - Y) \propto y^2$ represents the difference between the production of dissipation by self-stretching of vortex filaments P_ε^4 and the destruction of dissipation due to viscosity Y. Recently Jovanović et al.[42] proposed to express Ψ as a function of the stress anisotropy invariants in the framework of the homogeneous dissipation concept, satisfying the 2-C turbulence limit. For a fully developed nonrotating channel flow, this model function, evaluated from DNS data for anisotropy invariants,[41] shows excellent agreement with the DNS data for Ψ (Fig. 10c; symbols and dotted line, respectively). Moreover, Jovanović et al.[42] argue that this function should be universal, irrespective of the reasons for the stress anisotropy evolution. Figure 10c shows also the variation of Ψ for the axially rotating pipe flow, computed by the model of Jovanović et al. using the DNS data for stress anisotropy of Orlandi and Fatica.[6] Although the function does not explicitly contain any rotation parameter, Fig. 10c shows a clear increase in Ψ with the rotation rate. Unfortunately, the DNS data for $(P_\varepsilon^4 - Y)$, that is, Ψ, are not available for rotating flows, so that a direct comparison is not possible. However, an a priori evaluation from DNS data indicates that the Ψ function of Jovanović et al.[42] reproduces well the effect of rotation through the modification of the stress anisotropy. The models for Ψ, that is, $C_{\varepsilon 2}$ proposed by Bardina et al.[40] [Eq. (10)] and Hallbäck and Johansson[43] [Eq. (11)], resulted in a similar increasing tendency (not shown here).

Swirling Flows in Long, Straight Pipes

We considered two swirling flows entering long straight pipes, which were investigated experimentally by Kitoh[28] and Steenbergen.[29] In both cases, the profile of the tangential velocity component imposed at the pipe entrance corresponds to the so-called free vortex type. The only, but important, difference is in the swirl intensity,

$$S = 2\pi \int_0^R \frac{U W r^2 \, \mathrm{d}r}{\pi R^3 U_m^2}$$

For Kitoh's case $S = 1.0$, and for Steenbergen's case $S = 0.1$. Figures 6 and 11 show the Reynolds stress and mean velocity profiles at several selected cross sections downstream of the pipe inlet for the Steenbergen's case.

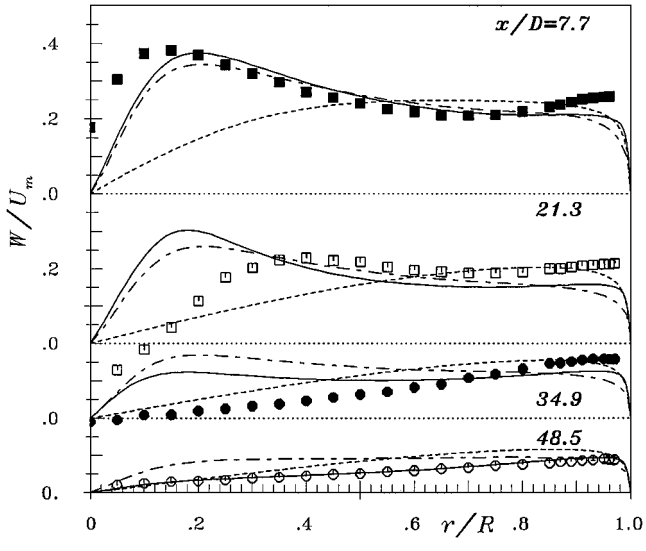

Fig. 11 Profiles of the tangential velocity components at selected positions in the swirling flow in a long, straight pipe, experiment of Steenbergen,[29] ----, low-Reynolds-number Chien k–ε, key as in Fig. 6.

Generally, the computational results obtained (except those with the Chien[32] low-Reynolds-number k–ε model) are in reasonable agreement with the experiments. In the annular region ($0.3 < r/R < 1.0$), there is a strong contribution of the negative gradient of the tangential velocity to the production of both normal-to-the-wall and spanwise stress components, so that these two stresses are much higher than in the nonswirling pipe flow. HJ low-Reynolds-number and SSG high-Reynolds-number second-moment closure computations reproduced this behavior very well (Fig. 6a). In the core region, however, up to the length of about $x/D = 35$, all three normal stress components show very high values, especially the wall-normal one. This flow region is characterized by a very high production rate (production plus convection): $P_{22} - C_{22} = 4\overline{vw}W/r$. In addition to a very strong radial gradient of the tangential velocity, the contribution of the axial swirl decay ($\partial U/\partial x > 0$, $\partial W/\partial x < 0$) is also significant. This region extends up to $x/D \approx 35$. Compared to the wall region, the agreement between computational and experimental results for turbulent stresses is poor, although both the axial (not shown here) and the tangential mean velocity components are well predicted. Approximately at this position, the flow evolves into a solid-body motion (Fig. 11), and the agreement is much better (Fig. 6b). This kind of transition is characteristic for the flows with a weaker swirl intensity, as in the case of Steenbergen's experiment[29] and because of this, these flows are very difficult to model. For the higher swirl intensities (Kitoh's experiment[28]), the flow remains of the free vortex type. The reason for the poor performance of the model in this region is probably because the mean shear $\partial U/\partial r$ and, consequently, the production rate P_{11} at the axis of symmetry become zero, whereas most of the models were calibrated in flows with a strong mean shear. The computations yield an almost isotropic stress field: $\overline{u^2} \approx \overline{v^2} = \overline{w^2}$. This behavior was also found in the computation of flow in a combustor chamber (experiment by So et al.[23]) by Hogg and Leschziner.[24] According to their conclusion, the simple linear formulation of the rapid part of the redistribution term is responsible for the underprediction of the normal Reynolds stress components. A similar conclusion was made by Kitoh,[28] who attributes this deficiency to a low value of the coefficient C_2 in the Launder–Reece–Rodi (LRR)[44] model. However, the application of the SSG model with a quadratic formulation of the rapid part brought no improvement, and, clearly, more detailed analysis is needed.

The transition of the free vortex flow type to solid-body rotation due to swirl decay has already been mentioned. The second-moment closures somewhat overpredicted the mean velocity profiles in the core region of the pipe at the position at which transition should occur $x/D \approx 35$. The velocity profiles retain their free vortex form, indicating a retarded decay of the swirl. The shear stress $\overline{uv}$ (Fig. 6) shows a direct proportionality to the gradient of the axial velocity (not shown here), with a change of the sign corresponding to the shape of the velocity profile. The wall-normal and spanwise stress components change the sign of the gradient also in accord with the observed velocity profiles. Similar, unrealistic velocity profiles, were obtained by Steenbergen[29] when applying an algebraic stress model. It is again believed that the linear model of the rapid part might be responsible for such a behavior. The performance of some cubic models for the rapid part (e.g., Fu and Wang[9]), having a stronger response to the streamline curvature (expressed in terms of additional straining $-W/r$, which has a very strong influence in the pipe core), are to be tested.

$\overline{uw}$ Anomaly

One of the perpetuating failures of all second-moment closures when applied to swirling and rotating flows is predicting the proper sign of the shear stress in the tangential plane, $\overline{uw}$. In the 1970s, Launder and Morse[45] in their computation of swirling free jets using an LRR quasi-isotropic (QI)[44] second-moment closure obtained the negative sign of $\overline{uw}$ in contrast to experimental results. This anomaly has been later confirmed by several subsequent computations in different swirling and rotating flows. For example, Oberlack et al.[15] recently reported the same problem in a fully developed channel flow with streamwise rotation when applying the SSG model in

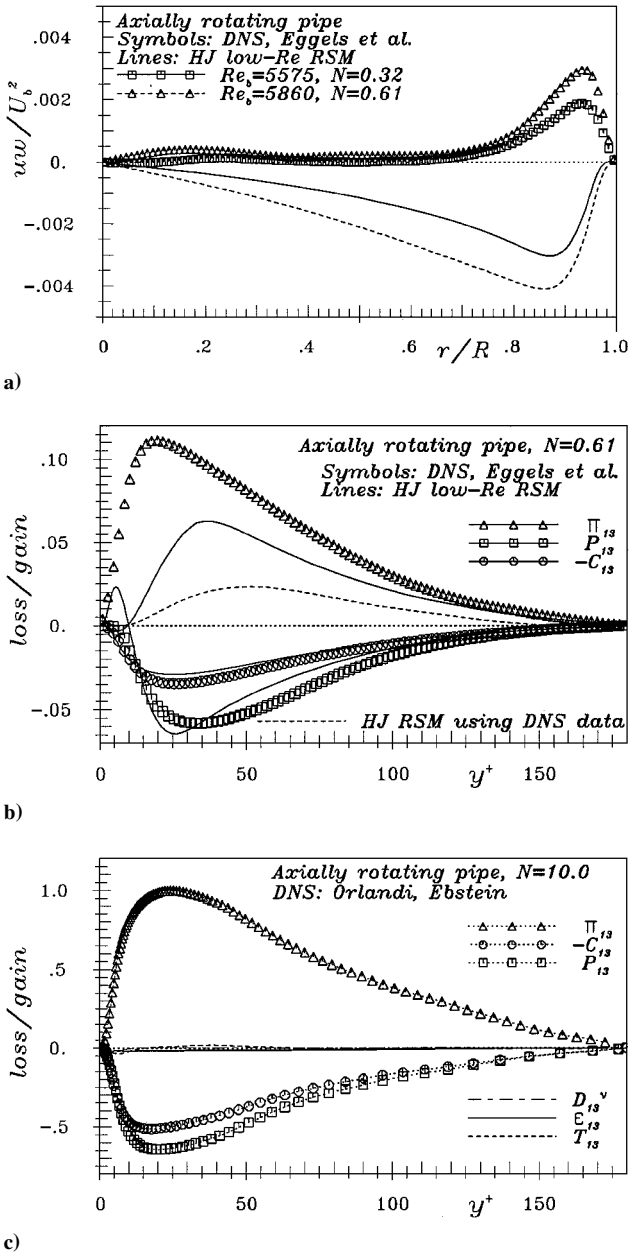

Fig. 12 Fully developed flow in an axially rotating pipe: comparison between the DNS data and results obtained by HJ low-Reynolds-number RSM for a) the $\overline{uw}$ shear stress; b) the pressure redistribution, production, and convection for $N = 0.61$; and c) DNS budget of the $\overline{uw}$ equation for $N = 10$.

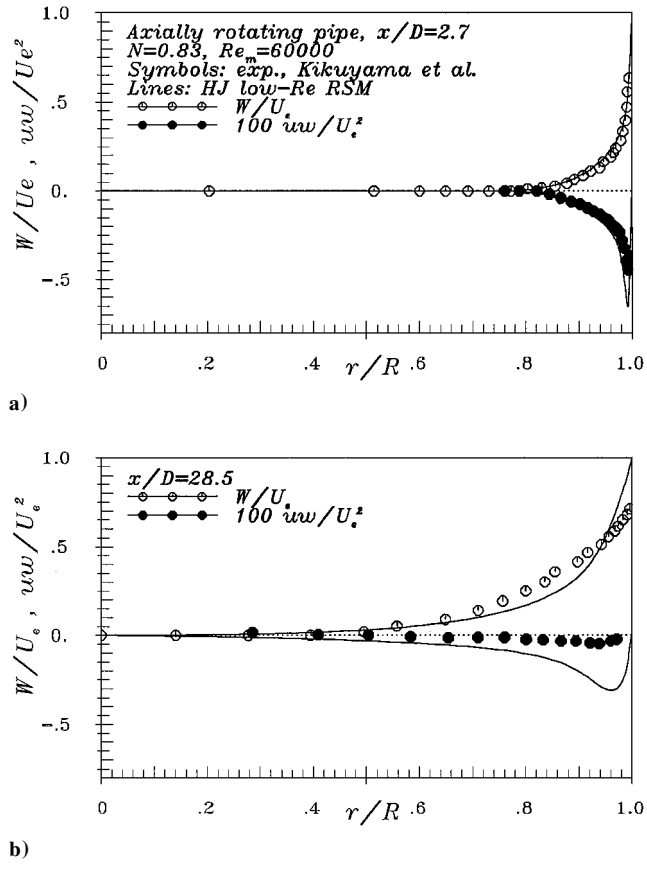

Fig. 13 Profiles of the tangential velocity and the shear stress $\overline{uw}$ in the developing flow in an axially rotating pipe.

conjunction with an elliptic relaxation method. [This was also confirmed by our computations using the Reynolds stress (RS) models considered here.]

We also obtained the negative $\overline{uw}$ in the axially rotating fully developed pipe flow, irrespective of the model type used (Fig. 12a), whereas the analysis of the exact equation for the stress $\overline{uw}$ (Eggels et al.[5]) suggests a positive sign. However, the opposite signs in predictions and experiments of $\overline{uw}$ seem to appear only in fully developed flows or not far from that condition. In the developing part of the flow in an axially rotating pipe studied experimentally by Kikuyama et al.,[1] the HJ second-moment closure yielded both the (negative) sign and amplitude in accord with experiments (Fig. 13a), but at the end of the rotating pipe (28.5D from inlet), where the conditions are very close to fully developed, the experiments show a tendency to change the sign (Fig. 13b). The negative sign was obtained also by Imao et al.[4] in their laser Doppler velocimetry measurements of the mean velocities and turbulent fluctuations in an axially rotating pipe. They concluded that a decrease in the U velocity and an increase in the W velocity in the radial direction (opposite signs of the velocity gradients $\partial U/\partial r$ and $\partial W/\partial r$) lead to opposite signs of their fluctuations u and w and, hence, the likely negative sign of their correlation $\overline{uw}$.

The origin of this anomaly is attributed to the inadequacy of the model of the pressure-strain term Φ_{13}, as seen in Fig. 12b. The (negative) production P_{13} $(= -\overline{vw}\,\partial U/\partial r - \overline{uv}\,\partial W/\partial r)$ and convection $-C_{13}$ $(= -\overline{uv}W/r)$, which balance the positive Φ_{13} in the equation for $\overline{uw}$ (see also Fig. 12c for very high rotation rate), are reproduced well in accord with the DNS results. Note that neither P_{13} nor C_{13} are explicitly influenced by the $\overline{uw}$. The model yields positive, but very much underpredicted, Φ_{13}. (Note that DNS data are shown for the velocity pressure gradient correlation Π_{13}, which differs from Φ_{13} only for the pressure diffusion term, here considered to be negligible in the bulk of the flow cross section.) The solid line shows the predictions using the full HJ model, that is, with computed negative $\overline{uw}$, whereas the broken line represents a priori evaluation of Φ_{13} using DNS data for all variables (including positive $\overline{uw}$) in the expression for the model of Φ_{13}. Therefore, irrespective of the sign of $\overline{uw}$, the model of Φ_{13} is unsatisfactory, and it is even worse when $\overline{uw} > 0$ from DNS is used. Because of negative production and convection, the underprediction of Φ_{13} results in negative $\overline{uw}$.

For the axially rotating pipe flow considered here, only data for the complete Φ_{ij} are available, and so it is not possible to diagnose precisely whether the main deficiency lies in its slow, rapid, or wall-reflection part. The simple linear model of the slow part $\Phi_{13,1} = -C_1\varepsilon\overline{uw}/k$ used here would imply that $\Phi_{13,1}$ should be negative, hence of an opposite sign from the total Φ_{13}. Application of the nonlinear formulation [Eq. (5)] in the framework of the SSG model and also in combination with the HJ low-Reynolds-number RSM did not result in any improvement. There is not much one can do to change the sign of the slow part because all model forms proposed in the literature (linear, quadratic) are based on a relatively sound hypothesis of return to isotropy of anisotropic turbulence in the absence of external forcing. This means that $\Phi_{13,1}$ is most probably negative, and the rapid part $\Phi_{13,2}$ should be positive and much larger than predicted by the GL and SSG models.

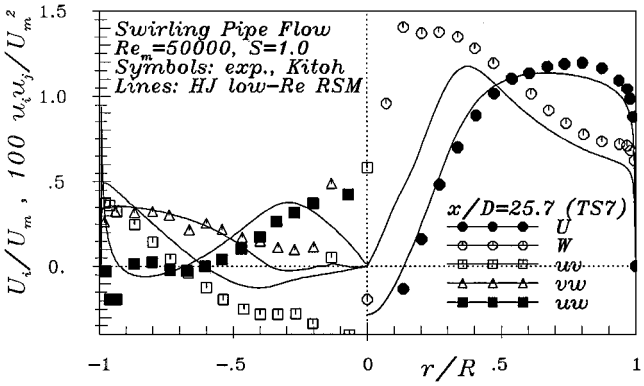

Fig. 14 Profiles of mean velocities and all three shear stress components on a selected position in the swirling flow in a long straight pipe with strong swirl.

Launder and Morse[45] associated the problem with the mean-strain contribution to Φ_{13} that is, with its rapid part $\Phi_{13,2}$. They used the QI model, so that the transport equation for $\overline{uw}$ ($C_{13} = P_{13} + \Phi_{13,1} + \Phi_{13,2}$) reduces to [practically identical for the isotropization of production (IP) formulation used in the GL model]

$$C_1 \frac{\varepsilon}{k}\overline{uw} = (\alpha - 1)\left(\overline{uv}\frac{\partial W}{\partial r} + \overline{vw}\frac{\partial U}{\partial r}\right) - (1+\beta)\overline{uv}\frac{W}{r} \qquad (9)$$

and succeeded in obtaining both the proper sign of the stress and its intensity in a free swirl flow, in reasonably good agreement with the experiments by reducing α by 40%. In the case of fully developed axially rotating pipe, such a remedy would have an opposite effect, that is, only an increase in the mean-strain contribution to the Φ_{13} would make $\overline{uw}$ positive. A numerical experiment, performed by the authors, confirmed this statement. However, because of a very weak influence of the $\overline{uw}$ stress on the mean flow and turbulence, the rate of amplification of the mean-strain effect needed to produce the desirable $\overline{uw}$ would be much higher compared to the experience of Launder and Morse.[45]

Figure 13 shows that the negative sign of the $\overline{uw}$-stress is closely connected to the positive gradient of the W velocity in the radial direction. For the flows in rotating pipes (Fig. 13), as well as in the flow regions with solid-body rotation (not shown here), this gradient is always positive (with relatively weak $\partial U/\partial r$ in this region), contributing to the negative production rate P_{13}. In the portions of cross section (annular regions) with the negative values of $\partial W/\partial r$, as in the Kitoh's[28] strongly swirling flow, the production rate P_{13} takes a positive value, leading to the positive $\overline{uw}$ stress (Fig. 14). In a part of this annular region with relatively weak strain rate contribution ($r/R \approx 0.85$), the $\overline{uw}$ stress takes a small negative value, being influenced mostly by additional production $-\overline{uv}W/r$ [see Eq. (9)]. Apart from larger scatter in the experimental data (in particular in the core region), all three shear stress components show reasonable agreement with measurements related to both their signs and amplitudes.

In the strongly swirling flow in a long straight pipe, Kitoh[28] observed a weak influence of this shear stress on the stress $\overline{uv}$ and consequently on the mean velocity field. In the fully developed flow in an axially rotating pipe, its influence is not so strong for lower rotation intensities ($N \leq 1.0$). The computations of these flows, with the stress $\overline{uw}$ taken from DNS, did not result in significant changes. However, the negative sign of this stress component causing negative production rate $P_{12} - C_{12}$ could significantly contribute to the premature laminarization at moderate and higher rotation rates.

From the preceding analysis it seems obvious that the inadequate modeling of the pressure scrambling process, and in particular of its rapid part $\Phi_{ij,2}$, is the main cause for wrong prediction of the $\overline{uw}$ stress. However, the application of more advanced models, such as SSG quadratic model, or cubic formulations by Fu, Launder, and Tselepidakis (see Ref. 9) and Ristorcelli, Lumley, and Abid, either in conjunction with the Durbin's elliptic relaxation method (see Ref. 11) or a structure-based model,[12] did not cure this anomaly, and the problem still awaits further clarification.

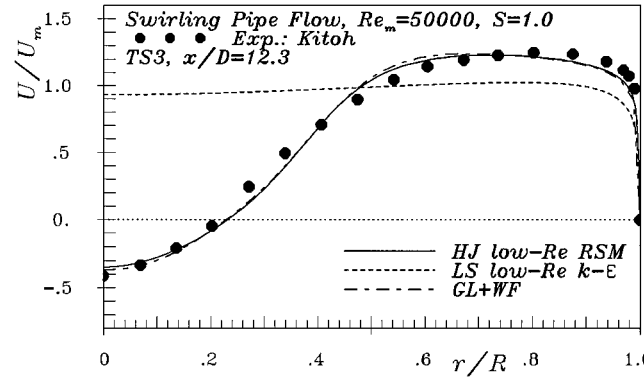

Fig. 15a Axial velocity profiles in the swirling flow in a long, straight pipe.

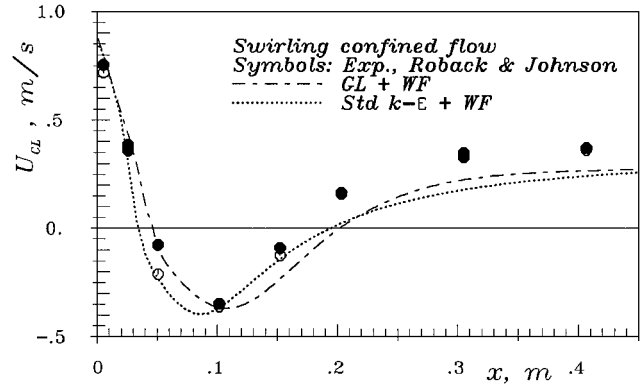

Fig. 15b Evolution of the centerline velocity along a combustor chamber with sudden expansion.

Comments on the k–ε Model

In the standard k–ε model, the k and ε equations are not directly sensitive to rotation and swirl because there are no specific terms accounting for these effects. Even in flows with system rotation (when considered in rotating frame of reference), the exact source term in the Reynolds stress equations R_{ij} contracts to zero and disappears from the kinetic energy equation. The same is true with the ε equation. Hence, both the k and ε equations retain the same form as in nonrotating and nonswirling flows. Of course, there are indirect effects due to the modification of the mean velocity and pressure field, but they are usually too weak to account fully for the effect of rotation and swirl on turbulence. This can be illustrated by the computational profiles of the axial velocity in an axially rotating pipe flow (not shown here) or in swirling flows in combustor chambers and long, straight pipes (Fig. 15a), which differ marginally from the nonrotating cases, irrespective of the rotation rate or the imposed initial conditions. One of the reasons for such a behavior is the simple linear relationship between Reynolds stress and the mean rate of strain tensors, implying essentially that the eddy viscosity is isotropic. However, it is well known that swirl causes a strong anisotropy of both the stress and dissipation tensors, as well as a highly anisotropic eddy viscosity (e.g., Kitoh[28]). This leads to the failure of all models based on the conventional linear eddy-viscosity concept. Another consequence of isotropic eddy viscosity is the "solid-body rotation" form of the tangential velocity profile (e.g., Fig. 11), which is always obtained, independent of the initial velocity profile. Associated with these features is the failure of the standard k–ε model to reproduce accurately the free recirculation zone encountered in flows in combustor chambers (in fact a swirling flow discharging into a sudden expansion; for example, see Lai[26]). However, note that in the case of higher expansion ratios (Lai investigated a case with $ER = 1.5$), for example, in the Roback and Johnson[22] experiment ($ER \approx 2.1$), good agreement relating to the length of this free vortex was obtained, also by the standard k–ε model (Fig. 15b). One possible explanation for this feature is that the superposition of the two flow phenomena, flow separation

and swirl, which are both incorrectly predicted by the k–ε models, results in a compensation.

Some improvements have been achieved with nonlinear eddy-viscosity formulations.[10] With these models, the tangential velocity does not follow the solid-body rotation pattern any more, but the models still do not properly account for the Reynolds stress anisotropy.

Model Modifications for Rotational Effects

Various modifications for rotational effects, proposed in the literature, are mostly related to the eddy-viscosity models to compensate for their insensitivity to system rotation. They are modeled in terms of rotational Richardson number (accounting for streamline curvature) and are usually introduced via additional term(s) in the scale supplying equation, that is, by modifying its model coefficients (e.g., Launder et al.[46] and Howard et al.[47]) or in the model for turbulent viscosity (Kim and Chung[48]). Recently, Shur et al.[49] introduced an empirical function multiplying the production rate in the eddy-viscosity transport equation of the Spalart–Allmaras model unifying in such a way the system-rotation and streamline-curvature effects.

Although there is no term in the exact dissipation rate equation that accounts directly for system rotation, ε is indirectly influenced through changes in anisotropies of the dissipation correlation ε_{ij}. The dynamic equation for the tensor ε_{ij} comprises a term governed by the angular velocity vector, similar to the transport equation for turbulent stresses. This confirms the necessity for the modification of the dissipation rate equation also in the framework of second-moment closure modeling, though here the problem is less acute: The exact rotation term R_{ij} in the stress equation accounts a great deal for the rotational effect on the stress anisotropy and indirectly to the dynamics of ε. However, for higher rotation rate this is not sufficient. Here we discuss some common modifications of the ε equation and their effects on the turbulence scale.

The major effect of system rotation is in reduction of the energy dissipation rate ε, due to the retardation of the energy transfer from large to small scales.[50] The change in ε naturally affects the turbulent stresses and the kinetic energy. Based on DNS and LES of rotating homogeneous turbulence, Bardina et al.[40] proposed the following modification of the dissipation destruction term, supposed to mimic the retardation of spectral energy transfer:

$$-C_{\varepsilon_2}\left(1 + C_{\varepsilon_\Omega}\Omega^*\right)(\varepsilon^2/k), \qquad \Omega^* = \Omega k/\varepsilon, \qquad C_{\varepsilon_\Omega} = 0.15/C_{\varepsilon_2} \tag{10}$$

The coefficient C_{ε_2} takes its standard value 1.92. Cambon et al.[51] pointed out that this modification leads to unrealistic nonzero k for larger decay times, contrary to the pure viscous decay at vanishing rotation numbers. Hallbäck and Johansson[43] confirmed the significant overprediction of k using the Bardina et al.[40] term, particularly in cases with high rotation rates. They proposed a new modification of the coefficient C_{ε_Ω} in terms of Reynolds number of turbulence $Re_t = k^2/(\nu\varepsilon)$:

$$C_{\varepsilon_\Omega} = \frac{0.6\sqrt{Re_t}}{C_{\varepsilon_2}(25 + 2\Omega^*)} \tag{11}$$

Shimomura[52] arrived at a similar conclusion. He also investigated the performance of the dissipation equation proposed by Hanjalić and Launder[53] for nonrotating flows, in which the term capturing the influence of irrotational straining on ε was introduced: $-2C_{\varepsilon_4}kW_{ij}W_{ij}$ ($C_{\varepsilon_4} = 0.27$). By transforming this term into a rotating frame of reference ($W_{ij} \to W_{ij} - \epsilon_{ijk}\Omega_k$), one obtains

$$-2C_{\varepsilon_4}kW_{ij}W_{ij} - 4C_{\varepsilon_4}k\Omega^2 + 4C_{\varepsilon_4}k\epsilon_{ijk}\frac{\partial U_i}{\partial x_j}\Omega_k \tag{12}$$

The analytical solution for k for homogeneous turbulent flow without mean shear ($\mathrm{D}k/\mathrm{D}t = -\varepsilon$) obtained by introducing this term into the dissipation equation ($\mathrm{D}\varepsilon/\mathrm{D}t = -C_{\varepsilon_2}\varepsilon^2/k - 4C_{\varepsilon_4}k\Omega^2$) yields a sinusoidal behavior causing negative values of ε. This formulation was made realizable by expressing the coefficient C_{ε_4} as a function of Ω^*. This remedy could finally be interpreted as a modification of the destruction term in the dissipation equation ($4C_{\varepsilon_4} \to C_{\varepsilon_\Omega}$):

$$-C_{\varepsilon_2}\left(1 + C_{\varepsilon_\Omega}\Omega^{*2}\right)(\varepsilon^2/k), \qquad C_{\varepsilon_\Omega} = 0.1/\left[C_{\varepsilon_2}\left(1 + 0.1\Omega^{*2}\right)\right] \tag{13}$$

This model formulation was shown to be superior to the Bardina et al.[40] model in computation of several homogeneous flow cases. Recently, Rubinstein and Zhou[54] proposed a further modification of the dissipation destruction term:

$$-C_{\varepsilon_2}\left(1 + C_{\varepsilon_\Omega}\Omega^{*2}\right)^{\frac{1}{2}}(\varepsilon^2/k) \tag{14}$$

This modification arose from the interpolation of the series expansions of the destruction term under the conditions of weak rotation (expansion in positive powers of Ω) and strong rotation (expansion in negative powers of Ω). No proposition for the coefficient C_{ε_Ω}, nor computational validation, were reported. Our test with model (14) did not produce the desirable improvement. In view of the fact that the rotational effects increase progressively with the rotation intensity, it seems more likely that an exponent in Eq. (14) should be higher than 1, instead of $\frac{1}{2}$, to capture the nonlinear rotational effects.

All modifications discussed were originally developed for the rotating homogeneous flows without mean rate of strain. Hence, they necessarily focus on the destruction term as the only existing term in the source of the ε equation. An increase in its magnitude in proportion to the rotation intensity will reduce ε and retard the decay of k as compared with the standard k–ε model, in accord with the DNS and experimental findings. However, for more general wall-bounded rotating and swirling flows, in which the rotation rate can vary with position, the effect of the modifications discussed is not so clear cut. Bardina et al.[40] argued that in such flows the magnitude of the system rotation vector $\boldsymbol{\Omega}$ [$= (\Omega_k\Omega_k)^{1/2}$] should be replaced by $(W_{ij}W_{ij}/2)^{1/2}$. However, such a term remains active also in flows without rotation, and it would deteriorate the predictions of flows that are well reproduced even by the standard k–ε or Reynolds stress (RST) models. In fact, introducing such a term resembles the earlier discussed proposal of Hanjalic and Launder,[53] who showed that inclusion of an additional term containing mean vorticity may be beneficial in nonequilibrium flows without rotation, but requires readjustment of other coefficient(s) to reproduce the canonic test cases in which the models are usually calibrated. This was also demonstrated by Jones and Pascau,[25] who showed that the Bardina et al.[40] term deteriorates significantly the prediction of a confined swirl flow as compared with the standard RST model. Hence, it can be concluded that these modifications are not very suitable for flows in the blade passages of turbomachinery, which are featured by a rotation-induced asymmetric influence on the turbulence. In spite of this, these terms have been used by some researchers supposedly to capture rotational effects (e.g., Jones et al.[55]).

Another model dissipation equation proposed by Shimomura[56] contains an additional source term $C_\Omega k\epsilon_{ijk}\partial U_i/\partial x_j\Omega_k$ with the coefficient $C_\Omega = 0.074$ being theoretically determined. Note that this term actually represents a part of the term proposed by Hanjalić and Launder[53] [Eq. (12)]. It is recalled here that some of the low-Reynolds number second-moment closures (e.g., Craft and Hanjalić and Jakirlić[35]) when applied to the computation of the rotating Poiseuille flow at relatively low bulk Reynolds numbers, for example, $Re_m \approx 6000$ by DNS of Kristoffersen and Andersson,[14] lead to premature flow laminarization[19] (private communication, T. J. Craft, 1998) as a consequence of the combined influence of viscosity and system rotation. This does not happen at higher bulk Reynolds numbers. See earlier section on rotating channel flows. Introduction of such a term prevents premature laminarization, but at the same time deteriorates the results for lower rotation numbers. As an illustration of its effect on the turbulent stresses, the computational results of the rotating Poiseuille flow by HJ low Reynolds number RSM, with addition of the Shimomura's[56] term with model coefficient enlarged to 0.12 are shown in Fig. 16. The value 0.12 is still too low to prevent the laminarization at the highest rotation number available, $Ro = 0.5$.

As in homogeneous flows, the addition of this term causes an increase in the destruction term of ε at the suction side. However, because of zero convection and negligible diffusion of k in fully developed channel flow, ε is completely in balance with the energy

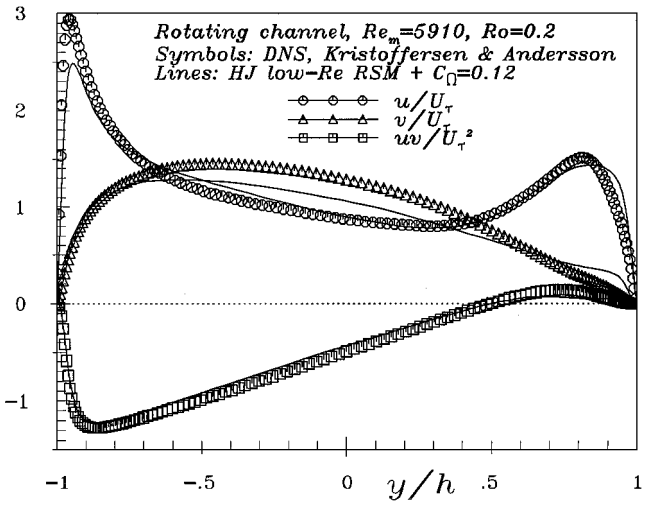

Fig. 16 Profiles of Reynolds stress components in the rotating Poiseuille flow obtained using Shimomura's[56] term ($C_\Omega = 0.12$).

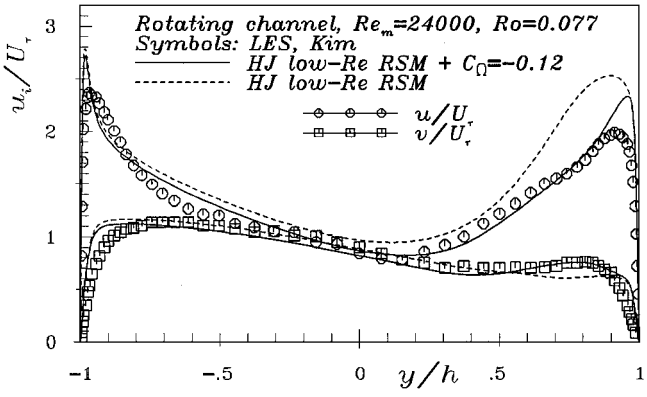

Fig. 17 Profiles of Reynolds stress components in the rotating Poiseuille flow; effect of Shimomura's[56] term ($C_\Omega = -0.12$).

production P_k. (Note that the molecular diffusion is influential only in the immediate wall vicinity for $y^+ \leq 2$.) Hence, unlike in homogeneous flows without production, here an increase in the destruction term of ε will lead also to an increase in ε and, consequently, to an increase in production rate of k in the largest portion of the flow cross section. This leads to an enhancement in the turbulence intensity, which prevents or delays the laminarization.

It is noted that, unlike other terms already discussed the term $\epsilon_{ijk}\partial U_i/\partial x_j$ differentiates the orientation of the rotation rate vector, modifying the turbulence energy selectively depending on the sign of the velocity gradient. For this reason, the term has often been used in the framework of different k–ε models and second-moment closures for rotating flows, for example, Shimomura,[56] Wizman et al.,[18] Pettersson and Andersson,[20] and Nagano and Hattori.[57] However, they all used a negative value of the coefficient C_Ω. This substantially increases the sensitivity of some models to the rotational effects. This is particularly the case when the k–ε modeling concept is employed. Without this term, completely symmetric profiles of mean and turbulence flow properties were obtained, (e.g., Nagano and Hattori[57]). The effect on turbulence is now opposite to the situation explained earlier, meaning that the turbulence level on the suction side will be reduced (Fig. 17). A slight enhancement of the wall-normal stress component is also captured, pointing to the effect of the isotropization of the near-wall turbulence due to rotation. (See Figs. 10a and 10b and corresponding explanation.)

We may conclude here, that despite the theoretical derivation of Shimomura,[56] a negative C_Ω yields the desired improvements in capturing asymmetric effects of rotation in rotating channel flows at higher Reynolds numbers. At low Reynolds numbers, a positive C_Ω would be more desirable to avoid premature laminarization, but this is probably the consequence of inappropriate modeling of the viscous effects.

IV. Conclusions

The potential of single-point turbulence closures for predicting the flow and turbulence in swirling and rotating confined flows was investigated by considering several flows with different rotation and swirl intensities and rotation vector orientation. The flows considered included short geometries (combustor chamber type) and long, straight pipes, fully developed and developing flows in axially rotating pipes, and flows in channels with streamwise and spanwise rotation.

The following general and specific conclusions have emerged:

1) The low-Reynolds-number version of the Reynolds stress model is superior to other models tested, particularly for flows in rotating pipes and for higher swirl intensities, where transition phenomena are observed. The major advantage of this model is its ability to capture the stress anisotropy in the near-wall region, which appears to be a necessary prerequisite for reproducing these types of flow.

2) The application of the standard k–ε high-Reynolds-number model and its low-Reynolds-number extensions in swirling and rotating pipe flows results in a solid-body rotation flow, thus failing to reflect important features of the flows considered.

3) Good agreement with experiment was found for the combustor geometry, whereas in long pipes, the swirl decay was somewhat too slow. For weak swirling flows, the circumferential velocity profiles remain too long of the free vortex type.

4) The negative sign of the shear stress $\overline{uw}$, obtained in (nearly) fully developed flows, is in contradiction with the DNS results. This has a very weak influence on other flow quantities for lower rotation rates. However, at higher rotation intensity, the negative $\overline{uw}$ causes negative production of the $\overline{uv}$ stress, leading eventually to the premature flow relaminarization.

5) A tendency toward laminarlike solutions for the flows in axially rotating pipes and channels with spanwise rotation was observed, particularly at lower bulk Reynolds numbers (based on axial velocity) and at higher rotation rates, indicating a need for further refinement of the dissipation equation.

6) The deficiency of wall functions becomes more pronounced when the swirl numbers that is, rotation rates increase. In general, if the flow is driven by the near wall phenomena, for example, friction, as in the rotating pipes and channels with both stationary and moving walls, and, in particular, if transition phenomena occurs, the wall function concept was proven to be totally unsuitable. If the extra strain rates causing nonequilibrium effects arise from the inner part of the flow as in swirling flows entering pipes or cylinders, and in particular, if the bulk Reynolds number is high, the wall function concept represents a reasonable alternative for treating wall boundaries.

Acknowledgments

We thank P. Orlandi and J. Eggels for making avaliable their DNS data for the fully developed flow in an axially rotating pipe. We are grateful for the numerous specific comments and suggestions from the reviewers.

References

[1]Kikuyama, K., Murakami, M., and Nishibori, K., "Development of Three-Dimensional Turbulent Boundary Layer in an Axially Rotating Pipe," *Journal of Fluids Engineering*, Vol. 105, June 1983, pp. 154–160.

[2]Nishibori, K., Kikuyama, K., and Murakami, M., "Laminarization of Turbulent Flow in the Inlet Region of an Axially Rotating Pipe," *Japan Society of Mechanical Engineers International Journal*, Vol. 30, No. 260, 1987, pp. 255–262.

[3]Hirai, S., Takagi, T., and Matsumoto, M., "Predictions of the Laminarization Phenomena in an Axially Rotating Pipe Flow." *Journal of Fluids Engineering*, Vol. 110, Dec. 1988, pp. 424–430.

[4]Imao, S., Itoh, M., and Harada, T., "Turbulent Characteristic of the Flow in an Axially Rotating Pipe," *International Journal of Heat and Fluid Flow*, Vol. 17, No. 5, 1996, pp. 444–451.

[5]Eggels, J. G. M., Boersma, B. J., and Nieuwstadt, F. T. M., "Direct and Large-Eddy Simulations of Turbulent Flow in an Axially Rotating Pipe," Lab. for Aero- and Hydrodynamics, Delft Univ. of Technology, Delft, The Netherlands, Oct. 1994.

[6]Orlandi, P., and Fatica, M., "Direct Simulations of Turbulent Flow in a Pipe Rotating about Its Axis," *Journal of Fluid Mechanics*, Vol. 343, 1997, pp. 43–72.

[7]Orlandi, P., and Ebstein, D., "Turbulent Budgets in Rotating Pipe by DNS," *International Journal of Heat and Fluid Flow*, Vol. 21, No. 5, 2000, pp. 499–505.

[8]Yoo, G. J., So, R. M. C., and Hwang, B. C., "Calculation of Developing Turbulent Flows in a Rotating Pipe," *Journal of Turbomachinery*, Vol. 113, Jan. 1991, pp. 34–41.

[9]Fu, S., and Wang, C., "Second-Moment Closure Modelling of Turbulence in a Non-Inertial Frame," *Fluid Dynamics Research*, Vol. 20, 1997, pp. 43–65.

[10]Shih, T.-H., Zhu, J., Liou, W. W., Chen, K.-H., and Lumley, J. L., "Modeling of Turbulent Swirling Flows," *Proceedings of the 11th Symposium on Turbulent Shear Flows*, 1997, pp. 31.1–31.6.

[11]Pettersson, B. A., Andersson, H. I., and Brunvoll, A. S., "Modeling Near-Wall Effects in Axially Rotating Pipe Flow by Elliptic Relaxation," *AIAA Journal*, Vol. 36, No. 7, 1998, pp. 1164–1170.

[12]Poroseva, S. V., Kassinos, S. C., Langer, C. A., and Reynolds, W. C., "Simulation of a Turbulent Flow in a Rotating Pipe Using the Structure-Based Model," *Proceedings of the 2nd Symposium on Turbulence and Shear Flows Phenomena*, 2001, pp. 149–154.

[13]Johnston, J. P., Hallen, R. M., and Lezius, D. K., "Effects of Spanwise Rotation on the Structure of Two-Dimensional Fully Developed Turbulent Channel Flow," *Journal of Fluid Mechanics*, Vol. 56, 1972, pp. 533–557.

[14]Kristoffersen, R., and Andersson, H., "Direct Simulations of Low-Reynolds-Number Turbulent Flow in a Rotating Channel," *Journal of Fluid Mechanics*, Vol. 256, 1993, pp. 163–197.

[15]Oberlack, M., Cabot, W. H., and Rogers, M. M., "Turbulent Channel Flow with Streamwise Rotation: Lie Group Analysis, DNS and Modeling," *Proceedings of the 1st Symposium on Turbulence and Shear Flows Phenomena*, 1999, pp. 85–90.

[16]Kim, J., "The Effect of Rotation on Turbulence Structure," *Proceedings of the 4th Symposium on Turbulent Shear Flows*, 1983, pp. 6.14–6.19.

[17]Launder, B. E., Tselepidakis, D. P., and Younis, B. A., "A Second-Moment Closure Study of Rotating Channel Flow," *Journal of Fluid Mechanics*, Vol. 183, 1987, pp. 63–75.

[18]Wizman, V., Laurence, D., Kanniche, M., Durbin, P., and Demuren, A., *Modeling Near-Wall Effects in Second-Moment Closures by Elliptic Relaxation, International Journal of Heat and Fluid Flow*, Vol. 17, No. 3, 1996, pp. 255–266.

[19]Jakirlić, S., Tropea, C., and Hanjalić, K., "Computations of Rotating Channel Flows with a Low-Re-Number Second-Moment Closure Model," 7th ERCOFTAC Workshop on Refined Flow Modelling, Univ. of Manchester Inst. of Technology, Manchester, England, U.K., May 1998.

[20]Pettersson, B. A., and Andersson, H. I., "Near-Wall Reynolds-Stress Modeling in Noninertial Frames of Reference," *Fluid Dynamics Research*, Vol. 19, 1997, pp. 251–276.

[21]Bech, K. H., and Andersson, H. I., "Turbulent Plane Couette Flow Subjected to Strong System Rotation," *Journal of Fluid Mechanics*, Vol. 347, 1997, pp. 289–314.

[22]Roback, R., and Johnson, B. V., "Mass and Momentum Turbulent Transport Experiments with Confined Swirling Coaxial Jets," NASA CR-168252, 1983.

[23]So, R. M., Ahmed, S. A., and Mongia, H. C., "An Experimental Investigation of Gas Jets in Confined Swirling Air Flow," NASA CR-3832, 1984.

[24]Hogg, S., and Leschziner, M., "Computation of Highly Swirling Confined Flow with a Reynolds Stress Turbulence Model," *AIAA Journal*, Vol. 27, No. 1, 1989, pp. 57–63.

[25]Jones, W. P., and Pascau, A., "Calculation of Confined Swirling Flows with Second Moment Closure," *Journal of Fluids Engineering*, Vol. 111, Sept. 1989, pp. 248–255.

[26]Lai, Y. G., "Predictive Capabilities of Turbulence Models for a Confined Swirling Flow," *AIAA Journal*, Vol. 34, No. 8, 1996, pp. 1743–1745.

[27]Chen, J. C., and Lin, C. A., "Computations of Strongly Swirling Flows with Second-Moment Closures," *International Journal for Numerical Methods in*, Vol. 30, 1999, pp. 493–508.

[28]Kitoh, O., "Experimental Study of Turbulent Swirling Flow in a Straight Pipe," *Journal of Fluid Mechanics*, Vol. 225, 1991, pp. 445–479.

[29]Steenbergen, W., "Turbulent Pipe Flow with Swirl," Ph.D. Dissertation, Eindhoven Univ., The Netherlands, 1995.

[30]Jakirlić, S., Tropea, C., Hadžić, I., Pascal, H., and Hanjalić, K., "Computational Study of Joint Effects of Shear, Compression and Swirl on Flow and Turbulence in a Valveless Piston-Cylinder Assembly," Society of Automotive Engineers, SAE Technical Paper 2001-01-1236, 2001.

[31]Launder, B. E., and Sharma, B. I., "Application of the Energy-Dissipation Model of Turbulence to the Calculation of Flow Near a Spinning Disc," *Letters in Heat and Mass Transfer*, Vol. 1, No. 2, 1974, pp. 131–138.

[32]Chien, K. Y., "Prediction of Channel and Boundary-Layer Flows with a Low-Reynolds-Number Turbulence Model," *AIAA Journal*, Vol. 20, No. 1, 1982, pp. 33–38.

[33]Gibson, M. M., and Launder, B. E., "Grounds Effects on Pressure Fluctuations in the Atmospheric Boundary Layer," *Journal of Fluid Mechanics*, Vol. 86, 1978, pp. 491–511.

[34]Speziale, C. G., Sarkar, S., and Gatski, T. B., "Modelling the Pressure–Strain Correlation of Turbulence: An Invariant Dynamical Systems Approach," *Journal of Fluid Mechanics*, Vol. 227., 1991, pp. 245–272.

[35]Hanjalić, K., and Jakirlić, S., "Contribution Towards the Second-Moment Closure Modeling of Separating Turbulent Flows," *Computers and Fluids*, Vol. 22, No. 2, 1998, pp. 137–156.

[36]Mayle, R. E., "The Role of Laminar-Turbulent Transition in Gas Turbine Engines," *Journal of Turbomachinery*, Vol. 113, Oct. 1991, pp. 509–537.

[37]Oberlack, M., "Generalized Theory for Symmetries in Inhomogeneous Turbulent Shear Flows," *Proceedings of the 11th Symposium on Turbulent Shear Flows*, 1997, pp. 10.21–10.26.

[38]Ferziger, J. H., and Shaanan, S., "Effect of Anisotropy and Rotation on Turbulence Production," *Physics of Fluids*, Vol. 19, No. 4, 1976, pp. 596–597.

[39]Hanjalić, K., Hadžić, I., and Jakirlić, S., "Modeling the Turbulent Wall Flows Subjected to Strong Pressure Variations," *Journal of Fluids Engineering*, Vol. 121, No. 1, 1999, pp. 57–64.

[40]Bardina, J., Ferziger, J. H., and Rogallo, R. S., "Effect of Rotation on Isotropic Turbulence: Computation and Modelling," *Journal of Fluid Mechanics*, Vol. 154, 1985, pp. 321–336.

[41]Kim, J., Moin, P., and Moser, R., "Turbulence Statistics in Fully Developed Channel Flow at the Low Reynolds Number," *Journal of Fluid Mechanics*, Vol. 177, 1987, pp. 133–166.

[42]Jovanović, J., Ye, Q.-Y., Jakirlić, S., and Durst, F., "Turbulence Closure for the Dissipation Rate Correlations," Lehrstuhl für Stroemungsmechanik, LSTM Rept. 618/T, Univ. of Erlangen–Nuremberg, Erlangen, Germany, Sept. 2001.

[43]Hallbäck, M., and Johansson, A. V., "Modelling of Rotation Effects in the ε-Equation and Reynolds Number Influence on Slow Pressure Strain in RST Closures," *Proceedings of the 5th International Symposium on Refined Flow Modelling and Turbulence Measurements*, 1993, pp. 65–72.

[44]Launder, B. E., Reece, G. J., and Rodi, W., "Progress in the Development of Reynolds-Stress Turbulence Closure," *Journal of Fluid Mechanics*, Vol. 68, 1975, pp. 537–566.

[45]Launder, B. E., and Morse, A., "Numerical Prediction of Axisymmetric Free Shear Flows with a Reynolds-Stress Closure," *Turbulent Shear Flows*, edited by L. J. S. Bradbury, F. Durst, B. E. Launder, F. W. Schmidt, and J. H. Whitelaw, Vol. 1, 1979, pp. 279–294.

[46]Launder, B. E., Priddin, C. H., and Sharma, B. I., "The Calculation of Turbulent Boundary Layers on Curved and Spinning Surfaces," *Journal of Fluids Engineering*, Vol. 99, March 1977, pp. 231–239.

[47]Howard, J. H. G., Patankar, S. V., and Bordynuik, R. M., "Flow Prediction in Rotating Ducts Using Coriolis-Modified Turbulence Models," *Journal of Fluids Engineering*, Vol. 102, Dec. 1980, pp. 456–461.

[48]Kim, K. Y., and Chung, M. K., "New Eddy Viscosity Model for Computation of Swirling Turbulent Flows," *AIAA Journal*, Vol. 25, No. 7, 1987, pp. 1020–1022.

[49]Shur, M., Strelets, M., Travin, A. K., and Spalart, P. R., "Turbulence Modeling in Rotating and Curved Channels: Assessing the Spalart–Shur Correction," *AIAA Journal*, Vol. 38, No. 5, 2000, pp. 784–792.

[50]Jacquin, L., Leuchter, O., Cambon, C., and Mathieu, J., "Homogeneous Turbulence in the Presence of Rotation," *Journal of Fluid Mechanics*, Vol. 220, 1990, pp. 1–52.

[51]Cambon, C., Jacquin, L., and Lubrano, J. L., "Toward a New Reynolds Stress Model for Rotating Turbulent Flows," *Physics of Fluids A*, Vol. 4, No. 4, 1992, pp. 812–824.

[52]Shimomura, Y., "Turbulence Modeling Suggested by System Rotation," *Near-Wall Turbulent Flows*, edited by R. M. C. So, C. G. Speziale, and B. E. Launder, Elsevier Science, New York, 1993, pp. 115–123.

[53]Hanjalić, K., and Launder, B. E., "Sensitizing the Dissipation Equation to Irrotational Strains," *Journal of Fluids Engineering*, Vol. 102, March 1980, pp. 34–40.

[54]Rubinstein, R., and Zhou, Y., "The Dissipation Rate Transport Equation and Subgrid-Scale Models in Rotating Turbulence," NASA CR-97-206250, ICASE, Rept. 97-63, Nov. 1997.

[55]Jones, R. M., Harvey, A. D., III, and Acharya, S., "Two-Equation Turbulence Modeling for Impeller Stirred Tanks" *Journal of Fluids Engineering*, Vol. 123, Sept. 2001, pp. 640–648.

[56]Shimomura, Y., "A Statistically Derived Two-Equation Model of Turbulent Flows in a Rotating System," *Journal of the Physical Society of Japan*, Vol. 58, Feb. 1989, pp. 352–355.

[57]Nagano, Y., and Hattori, H., "An Improved Turbulence Model for Rotating Shear Flows," *Proceedings of the 2nd Symposium on Turbulence and Shear Flows Phenomena*, Vol. 2, 2001, pp. 199–205.

R. M. C. So
Associate Editor